Article

pubs.acs.org/Biomac

Holocellulose Nanocrystals: Amphiphilicity, Oil/Water Emulsion, and Self-Assembly

Feng Jiang and You-Lo Hsieh*

Fiber and Polymer Science, University of California, Davis, California 95616, United States

Supporting Information

ABSTRACT: Amphiphilic holoCNCs were derived from rice straw holocellulose by sulfuric acid hydrolysis (64%, 45 °C, 45 min) at 11.6% yield (8.8% of rice straw). HoloCNCs are similar in lateral dimensions (4.1 ± 1.6 nm thick, 6.4 ± 1.8 nm wide), but shorter and more heterogeneous in lengths (113 ± 70 nm long), less negatively charged (0.128 mmol/g) and less crystalline (CrI 84.4%) than CNCs. HoloCNCs were also more thermally stable (T_{max} =284 °C), attributed to the presence of residual lignosulfonate, hemicellulose, and silica. Most remarkable, the amphiphilic holoCNCs were more hydrophobic than CNCs, exhibiting distinct surface active behaviors and lowering equilibrium surface tension to 49.2 mN/m at above 0.57% critical aggregation concentration. HoloCNCs not only stabilize 30% more oil-in-water (O/W) emulsion and formed droplets (1.2−1.6 μm) doubled the sizes of those with CNCs, but also self-assembled into highly mesoporous structures with up to 3× higher specific surface (111 m^2/g) and total pore volume (0.40 cm^3/g) than that from CNCs upon freeze-drying. The unique surface active, amphiphilic, and less self-assembling properties of holoCNCs offer new desirable characteristics but without additional isolation process nor surface modification of CNCs.

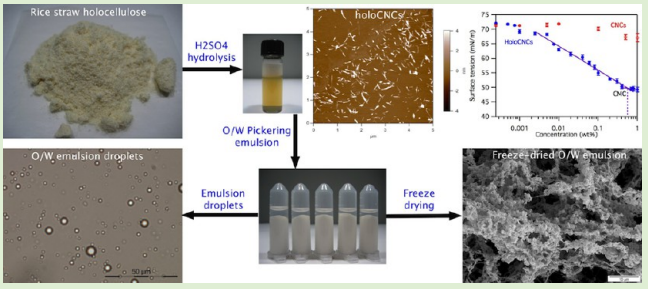

INTRODUCTION

Cellulose nanocrystals (CNCs) are highly crystalline nanorods with 2−20 nm lateral dimensions and 100 nm to several micrometer lengths,[1−4] commonly derived from acid hydrolysis of cellulose.[5,6] CNCs have attracted tremendous interests due to its unique properties including high crystallinity of over 90%,[7,8] extraordinary elastic modulus of 110−220 GPa[4,9,10] and outstanding tensile strength of 2−6 GPa.[11] CNCs reported to date have focused primarily on those hydrolyzed from purified cellulose from sources such as bleached wood pulp,[5,12] bacteria,[13] cotton,[14,15] tunicate,[16,17] microcrystalline cellulose,[18] as well as agricultural residues, including rice straw[8,19] and husk,[20] grape pomace,[21] wheat straw,[22] tomato[23] and potato[24] peels, banana plants,[25] and so on.

As cellulose microfibrils are tightly embedded in lignin and hemicellulose matrixes,[26,27] isolation of pure cellulose requires intensive chemical and energy input. Therefore, CNCs and cellulose nanofibrils (CNFs) have also been isolated from less purified lignocellulosics, such as mechanically defibrillated wood pulp containing varying amounts of lignin and hemicellulose,[28−30] hemp fibers,[31,32] softwood thermomechanical pulp,[33,34] and hardwood kraft pulp,[35] as well as holocellulose from softwood, hardwood and rice straw,[36] bagasse pulp,[37] and coconut fibers.[38] While in 2,2,6,6-tetramethylpiperidine-1-oxyl (TEMPO) mediated oxidation most hemicellulose in softwood, hardwood, and herbaceous holocellulose,[32,36] as well as lignin in hemp fibers[31] and softwood thermomechanical pulp[33,34] were degraded to become water-soluble and removed, sulfuric acid hydrolysis of bagasse pulp containing 27% hemicellulose[37] and partially delignified coconut fibers[38] has shown to leave some noncellulosics with CNCs. The presence and effects of the residual hemicellulose and lignin on the isolated nanocrystals have, however, not been clearly delineated.

This study focused on structural elucidation of holocellulose nanocrystals (holoCNCs) from the less pure holocellulose by sulfuric acid hydrolysis. Holocellulose was isolated from rice straw following the previously established three-step dewax-delignification-alkaline leaching procedure for pure cellulose[8] by omitting the third alkaline step, then hydrolyzed to holoCNCs by sulfuric acid. HoloCNCs were characterized in terms of dimensions, chemical and crystalline structures, thermal stabilities, surface active properties, ability to stabilize Pickering emulsions, and self-assemble to discern the effects of noncellulosic components on holoCNCs and to compare with CNCs derived from pure rice straw cellulose. Deriving holoCNCs from holocellulose is attractive from the perspective of reduced isolation process, thus, reduced chemical and energy consumption, as well as potential utilization of the noncellulosics. Furthermore, the presence of residual noncellulosics on holoCNC surfaces may offer novel surface properties that currently have to be acquired by chemical modification of CNCs via surfactant adsorption,[39,40] periodate oxidation and

Received: February 19, 2015
Revised: March 11, 2015
Published: March 16, 2015

DOI: 10.1021/acs.biomac.5b00240
Biomacromolecules 2015, 16, 1433−1441

reductive amination with butylamine,[41] grafting of poly[2-(dimethylamino)ethyl methacrylate][42] and Jeffamine,[43] and so on.

EXPERIMENTAL SECTION

Materials. Holocellulose was isolated from rice straw (Calrose variety) by 2:1 v/v toluene/ethanol extraction of organic solubles and acidified $NaClO_2$ dissolution of lignin (1.4%, 70 °C, 5 h) whereas α-cellulose was obtained by including a third step of alkaline dissolution of hemicellulose and silica (5% KOH, 90 °C for 2 h), latter as previously reported.[8] The yields of holocellulose and α-cellulose were determined gravimetrically and reported as percentages of the original rice straw. Sulfuric acid (H_2SO_4, 95−98%, ACS GR, EMD), hydrochloric acid (HCl, 1 N, certified, Fisher Scientific), sodium hydroxide (NaOH, 1 N, certified, Fisher Scientific), and *n*-hexadecane (certified, Fisher Scientific) were used as received without further purification. All water used was purified by Milli-Q plus water purification system (Millipore Corporate, Billerica, MA).

Isolation of Holocellulose Nanocrystals (holoCNCs) and Cellulose Nanocrystals (CNCs). Holocellulose and α-cellulose were added to preheated (45 °C) sulfuric acid (64 w/w%) at a 8.75 mL/g acid-to-cellulose ratio and proceeded at 45 °C under constant stirring for 45 min, followed by centrifugation and dialysis to remove the residual acids, yielding holoCNCs and CNCs, respectively.[19] The solids from centrifugation were dried and weighed to be subtracted from the original holocellulose and cellulose to determine the yield. The gravimetrically determined holoCNC and CNC yields were reported as percentages based on the respective holocellulose and α-cellulose, as well as the starting rice staw. All concentrations of aqueous holoCNCs and CNCs were w/w percentages and reported simply as % throughout.

Characterization of Aqueous HoloCNCs and CNCs. The surface charges of both holoCNCs and CNCs were determined from conductivity measurement by titrating 50 mL of 0.1% suspension with 0.005 M NaOH using OAKTON pH/Con 510 series meter. The optical transmittance and UV−vis absorbance spectrum of aqueous holoCNC and CNC suspensions were recorded at 0.2 and 0.025% concentrations, respectively, from 200 to 900 nm using Evolution 600 UV−vis spectrophotometer (Thermo Scientific) in quartz cuvette. AFM sample was prepared by depositing 10 μL of 0.0005% suspension onto a freshly cleaved mica surface and air-dried, then scanned at 1 Hz rate and 512 × 512 pixels image resolution under ambient condition using an Asylum-Research MFP-3D atomic force microscope in the tapping mode with OMCL-AC160TS standard silicon probes. The height profiles were determined with MFP3D 090909 + 1409 plugin in IGOR Pro 6.21 and the average heights reported. TEM specimens were prepared by depositing 10 μL of 0.001% suspension onto glow-discharged carbon-coated TEM grids (300-mesh copper, Formvar-carbon, Ted Pella Inc., Redding, CA), and the excess liquid was removed by blotting with a filter paper after 10 min. The specimens were then negatively stained with 2% uranyl acetate solution for 5 min, blotted, dried under the ambient condition and observed using a Philip CM12 transmission electron microscope operated at a 100 kV accelerating voltage. The lengths and widths of holoCNCs and CNCs were measured and calculated from over 200 samples using analySIS FIVE software. The surface tensions of aqueous holoCNC and CNC suspensions at concentrations ranging from 0.0025 to 1% were determined by the Wilhelmy plate method using a tensiometer (K100, Kruss GmbH, Germany). The platinum plate was thoroughly rinsed after each measurement with DI water and dried under filtered compressed air stream. At least three measurements were conducted at each concentration and the average value and standard deviation were reported. The fluorescence emission spectra of pyrene (10^{-5} M) probe in aqueous holoCNC and CNC suspensions at 0.0001 to 0.2% concentrations was recorded from 360 to 500 at 334 nm excitation wavelength by steady-state fluorescence spectrometer (PerkinElmer LS 50 fluorescence spectrometer, Waltham, MA). The slit settings for excitation and emission were 5 and 2.5 nm, respectively. CNC and holoCNC suspensions containing pyrene were prepared by dissolving pyrene in ethanol at 10^{-3} M, and then aliquots of the pyrene solution were measured into glass vials and dried. Upon evaporation of ethanol, aliquots of CNC and holoCNC suspensions were measured into the vials to 10^{-5} M Pyrene concentration.

Characterization of Freeze-Dried HoloCNCs and CNCs. Aqueous holoCNC and CNC suspensions (0.1%) were frozen in liquid nitrogen (−196 °C) and lyophilized at −50 °C in a freeze-drier (FreeZone 1.0L Benchtop Freeze-Dry System, Labconco, Kansas City, MO). Elemental analysis was conducted using EDS (EDAX, AMETEK, Inc.) on the scanning electron microscope at 350× magnification with 10 kV accelerating voltage and 5 mm working distance. FTIR spectra of holoCNCs and CNCs as transparent KBr pellets (1:100, w/w) were obtained from a Thermo Nicolet 6700 spectrometer under ambient conditions from an accumulation of 128 scans at a 4 cm^{-1} resolution from 4000 to 400 cm^{-1}. TGA were performed on a TGA-50 thermogravimetric analyzer (Shimadzu, Japan) by heating 5 mg sample at 10 °C/min from 25 to 500 °C under purging N_2 (50 mL/min). XRD spectra were collected on a Scintag XDS 2000 powder diffractometer using a Ni-filtered Cu Kα radiation (λ = 1.5406 Å) at an anode voltage of 45 kV and a current of 40 mA from 5° to 40° at a scan rate of 2°/min. Crystallinity index (CrI) was calculated from the intensity of the 200 peak (I_{200}, 2θ = 22.6°) and the intensity minimum between the peaks at 200 and 110 (I_{am}, 2θ = 18.7°) by using the empirical equation.[44]

$$\mathrm{CrI} = \frac{I_{200} - I_{am}}{I_{200}} \times 100 \quad (1)$$

Oil-in-Water O/W Pickering Emulsion. Each O/W Pickering emulsion was prepared by adding hexadecane (0.45 mL) into either aqueous holoCNC or CNC suspension (1.05 mL) at varying concentrations of 0.01, 0.05, 0.1, 0.2, and 0.3%, followed by sonication (Branson 2510) for 30 min and let settled for 30 min. The top clear oil layer was carefully removed and its volume was subtracted from 0.45 mL, the initial oil volume, to give the emulsified volume in the suspension. The extent of emulsion was calculated from dividing the emulsified volume by the initial oil volume.

Droplet sizes in the Pickering emulsions were measured by both optical light microscopy and dynamic light scattering. Each emulsion was diluted by adding 100 μL of emulsion into 10 mL water and hand shaken to homogeneous dispersion from which a drop (10 μL) was deposited on a glass slide and covered with a cover slide to be observed by an optical microscope (Leica DM2500). Over 50 individual droplets were measured for each emulsion using ImageJ software (http://rsbweb.nih.gov/ij/) to determine the average droplet size. The emulsion droplet sizes were also determined using dynamic light scattering (Zetasizer Nano S90, Malvern Instruments, Ltd.) in triplicates.

Both holoCNC and CNC O/W emulsions (0.2%), with excess oil being removed, were frozen in liquid nitrogen (−196 °C) and lyophilized at −50 °C in a freeze-drier. The freeze-dried samples were sputter coated with gold and visualized using a field emission scanning electron microscope (FE-SEM; XL 30-SFEG, FEI/Philips, U.S.A.) at a 5 mm working distance and 5 kV accelerating voltage. The specific surface and pore characteristics of degassed (35 °C for 24 h) samples were determined by N_2 adsorption and desorption isotherms at 77 K using a surface area and porosity analyzer (ASAP 2000, Micromeritics, U.S.A.) and the Brunauer−Emmett−Teller (BET) method.[45] Pore size distributions were derived from desorption branch of the isotherms by the Barrett−Joyner−Halenda (BJH) method.[46] The total pore volumes were estimated from the amount adsorbed at a relative pressure of P/P_0 = 0.98.

Cast HoloCNC and CNC Films. Free standing holoCNC and CNC films were casted from 5 mL of 2% aqueous suspensions in polystyrene weighing dishes (Fisher brand, Fisher Scientific) at 65 °C until dried. The films were observed under a Leica DM2500 optical microscope equipped with cross polarized filter as well as scanned using an Asylum-Research MFP-3D atomic force microscope under ambient condition in the tapping mode with OMCL-AC160TS

DOI: 10.1021/acs.biomac.5b00240
Biomacromolecules 2015, 16, 1433−1441

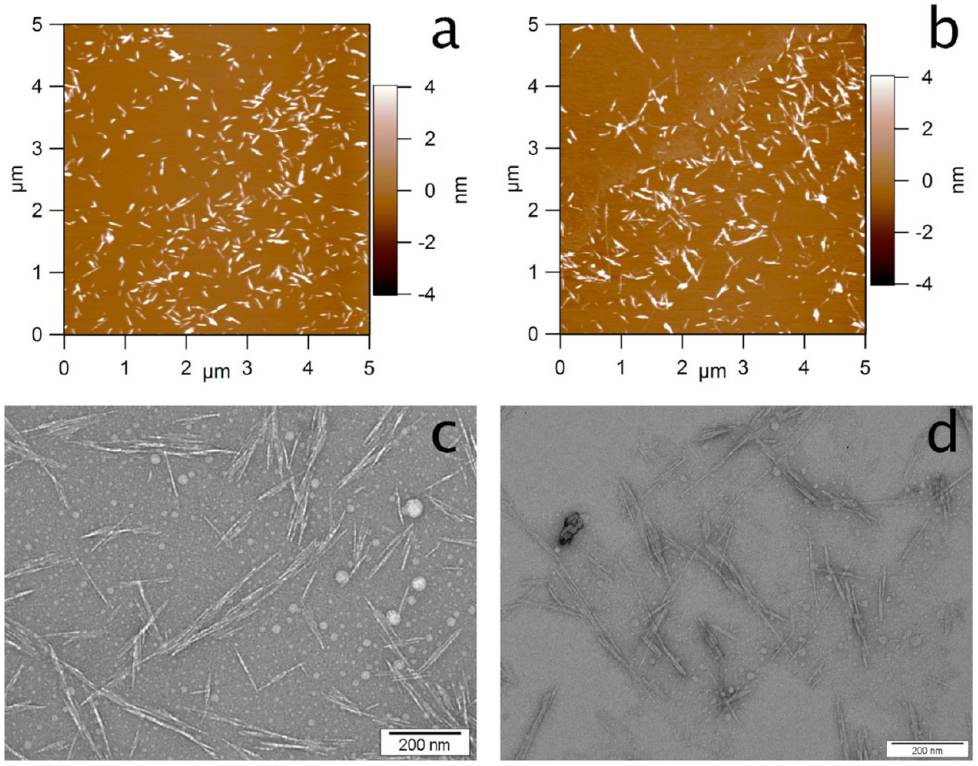

Figure 1. AFM (a, b) and TEM (c, d) images of CNCs (a, c) and holoCNCs (b, d).

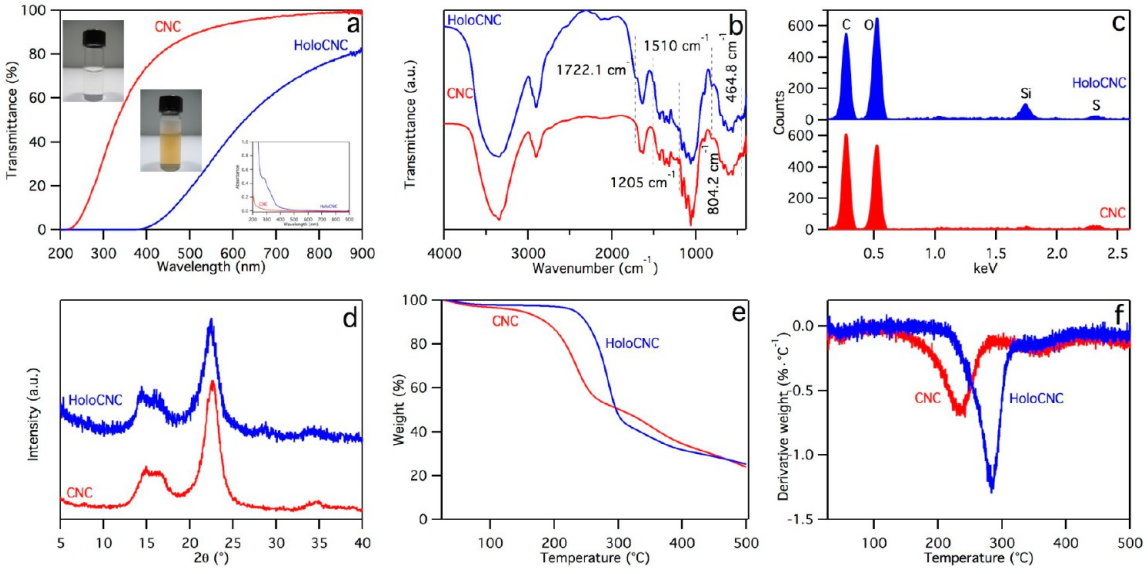

Figure 2. Characterization of CNCs and holoCNCs: (a) light transmittance of 0.2% aqueous suspensions, (b) FTIR, (c) EDS, (d) XRD, (e) TGA, and (f) DTGA spectra of frozen (−196 °C) and lyophilized (−50 °C) CNCs and holoCNCs, inset in (a) are 0.2% CNC and holoCNC after hand shaking, as well as the UV−vis spectra of 0.025% CNC and holoCNC suspensions.

standard silicon probes at 1 Hz scan rate and 512 × 512 pixels image resolution.

RESULTS AND DISCUSSION

Isolation and Characterization of HoloCNCs and CNCs. Holocellulose and α-cellulose were isolated from rice straw at 75.4 and 36.4% yields, respectively. The structure of α-cellulose was confirmed by FTIR to be pure cellulose whereas holocellulose showed strong carbonyl stretching at 1732 cm^{-1} and Si−O−Si stretching at 785 and 471 cm^{-1} (Figure S1a, Supporting Information),[8] evident of significant hemicellulose and silica that accounted for the 39% higher holocellulose mass than that of α-cellulose. Holocellulose decomposed at a lower onset temperature of 260 °C than α-cellulose (300 °C) and a much lower maximum 0.9%/°C mass loss rate at 346 °C as compared to the 2.6%/°C mass loss rate at 361 °C for α-cellulose, but a significantly higher 32.3% residue than the 3.3% for α-cellulose at 500 °C (Figure S1b in Supporting Information). The lower degradation temperature of holocellulose is consistent with the presence of hemicellulose, whereas

DOI: 10.1021/acs.biomac.5b00240
Biomacromolecules 2015, 16, 1433−1441

both hemicellulose and silica could contribute to the much higher residues.

Upon sulfuric acid hydrolysis (64%, 45 °C, 45 min), holocellulose nanocrystals (holoCNCs) and cellulose nanocrystals (CNCs) were isolated at 11.6 and 6.8% yields of holocellulose and α-cellulose or 8.8 and 2.5% of rice straw, respectively. The 3.5× higher holoCNCs yield than that of CNCs could be attributed to the less hydrolyzed cellulose and possibly residual hemicellulose and silica. In hydrolyzing α-cellulose, very little residual solid was observed after separating CNCs, indicating most cellulose has been hydrolyzed into soluble oligosaccharides, glucose, and possibly other small molecules. In contrast, the same hydrolysis of holocellulose left significant 33.5% residual solid whose FTIR showed clear evidence of cellulose, hemicellulose, and silica (Figure S2a in Supporting Information). EDS of the solid residue also showed the presence of 26.6 wt % or 15.2 atom% of silicon, corresponding to 14.4 wt % silica in the rice straw (Figure S2b in Supporting Information). Based on the 13−14 wt % silica content reported for rice straw,[47,48] almost all silica in the original rice straw would have been left in the precipitate. In other words, very little silica is expected to remain within holoCNCs.

Both holoCNCs and CNCs were rod-like as clearly shown in the AFM and TEM images (Figure 1), confirming successful isolation of individual crystallites in both cases. The average thickness, width, and length of holoCNCs were 4.1 ± 1.6, 6.4 ± 1.8, and 113 ± 70 nm, respectively, similar in lateral dimensions but shorter and more heterogeneous in lengths than CNCs (4.7 ± 1.3, 6.4 ± 1.2, and 143 ± 31 nm). The similarity in dimensions of CNCs and holoCNCs suggested the morphologies of sulfuric acid hydrolyzed nanocrystals are less dependent on the pretreatment of the raw materials. During hydrolysis with strong sulfuric acid, the less ordered and bound lignocellulosic structures were degraded, leaving highly crystalline cellulose. As both CNCs and holoCNCs were derived from the same rice straw with the same cellulose crystalline structures and dimensions, their similar morphologies showed the presence of noncellulosics did not interfere with hydrolysis.

Aqueous holoCNC suspension (0.2%) appeared brownish and showed zero transmittance between 200 and 400 nm and increasing transmittance with wavelength in the visible region (Figure 2a). This is in contrast to the nearly clear aqueous CNC suspension that transmitted over 74% from 400 to nearly 100% at 900 nm, showing little to no absorption and scattering in the visible light region. For holoCNCs, even the diluted 0.025% suspension showed strong absorbance between 200 and 400 nm with a small peak at 280 nm (inset, Figure 2a), consistent with the absorption peak for the aromatic ring of lignosulfonate,[49−51] a hydrolysis product of residual lignin in holocellulose. Therefore, the presence of lignosulfonate in holoCNCs is evident. Most distinctively, aqueous holoCNC suspensions foamed upon shaking (inset, Figure 2a), indicating holoCNCs to be surface active at the air/water interface. The foams could persist for hours and such behavior is elaborated further later.

The presence of lignosulfonate in holoCNCs was further confirmed by the small FTIR peak at 1510 cm^{-1} attributed to aromatic skeletal vibrations. HoloCNCs also exhibited additional hemicellulose (C═O stretching at 1722.1 cm^{-1}) and silica (Si−O−Si stretching at 804.2 and 464.8 cm^{-1}) characteristic peaks, whereas the FTIR spectrum of CNCs was typical of cellulose (Figure 2b). Both holoCNCs and CNCs exhibited small peaks at 1205 cm^{-1}, indicative S═O stretching of sulfate groups.[14]

Both holoCNCs and CNCs were negatively charged at 0.128 and 0.237 mmol/g, respectively, as determined by conductometric titration. The EDS spectra of both CNCs and holoCNCs showed S peaks at 0.7 and 0.6 atom%, respectively (Figure 2c), confirming the presence of sulfate groups on both. Since EDS is semiquantitative, surface charge determined by conductometric titration was deemed more accurate to represent the surface nature of holoCNCs and CNCs. HoloCNCs contain around one-half of negative charge groups compared to CNCs, even considering the presence of lignosulfonate on holoCNCs, indicating less sulfated surfaces due to the presence of lignin/hemicellulose and silica that consumed the acid as well as impeded its access to cellulose. Besides, 2.5 atom% or 4.96 wt % silicon was observed on holoCNCs, translating to 10.6 and 0.93 wt % silica in the respective holoCNCs and rice straw. Together with the 14.4% silica determined in the precipitates from acid hydrolysis, the total silica content in rice straw is estimated to be 15.33%. In other words, over 94% of silica in rice straw was precipitated during acid hydrolysis, and the remaining in holoCNCs.

XRD spectra of both CNCs and holoCNCs showed characteristic cellulose Iβ peaks at 14.7, 16.8, and 22.7° (Figure 2d), corresponding to the $1\bar{1}0$, 110, and 200 crystallographic planes of the monoclinic lattice, respectively.[6] HoloCNCs were slightly less crystalline than CNCs, that is, at respective 84.4% and 90.7% CrI, but both higher than the 72.2% CrI of rice straw cellulose. The slightly lower crystallinity of holoCNCs is attributed mainly to the presence of hemicellulose, lignosulfonate and silica and possibly retention of the less crystalline cellulose.

HoloCNCs decomposed over 214−323 °C temperature range and reached 1.3%/°C maximum mass loss rate at 284 °C whereas CNCs decomposed over a lower 160 to 280 °C range at a much lower maximum 0.7%/°C rate at 235 °C (Figure 2e,f). The maximum mass loss temperature for both CNCs (235 °C) and holoCNCs (284 °C) are lower than those of α-cellulose (361 °C) and holocellulose (346 °C) precursors, possibly due to the lowered activation energy of decomposition from the surface sulfate groups.[13,14,19] The higher decomposition temperature of holoCNCs could be attributed to the lower sulfate content or less sulfonated surfaces and the presence of the more thermally stable lignosulfonate and silica. The char residues at 500 °C were, however, similar for holoCNCs and CNCs, that is, at 25.3 and 23.8%, respectively. Both CNCs and holoCNCs also showed the same small peaks at 360 °C in their DTGA curves, primarily from the breakdown of charred residues to gaseous products.[13] Therefore, although holoCNCs and CNCs decompose in different rates initially, their gasification and charring processes were similarly, balanced by the higher sulfate contents in CNCs and the more thermally stable lignin and silica in holoCNCs.

Amphiphilic Properties of HoloCNCs and CNCs. The foaming behavior of holoCNCs observed earlier suggested more distinct amphiphilicity and was further investigated by steady-state fluorescence of pyrene as fluorescent probe in varying concentrations of holoCNCs and CNCs. In pyrene emission spectrum, the ratio of the first and third vibrational peak intensities (I_1/I_3) indicates the polarity of the probe microenvironment,[52] that is, a higher I_1/I_3 value indicates a more polar microenvironment and vice versa. For instance, the

DOI: 10.1021/acs.biomac.5b00240
Biomacromolecules 2015, 16, 1433−1441

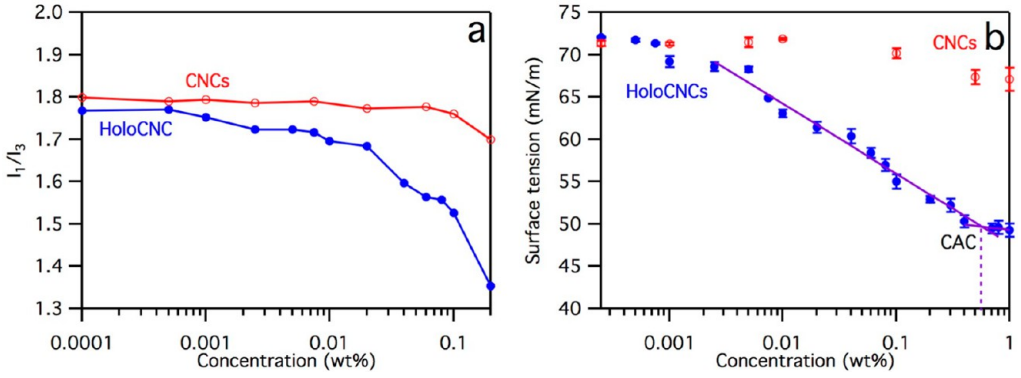

Figure 3. Aqueous CNCs and holoCNCs suspensions: (a) I_1/I_3 ratio of pyrene emission spectrum and (b) surface tension.

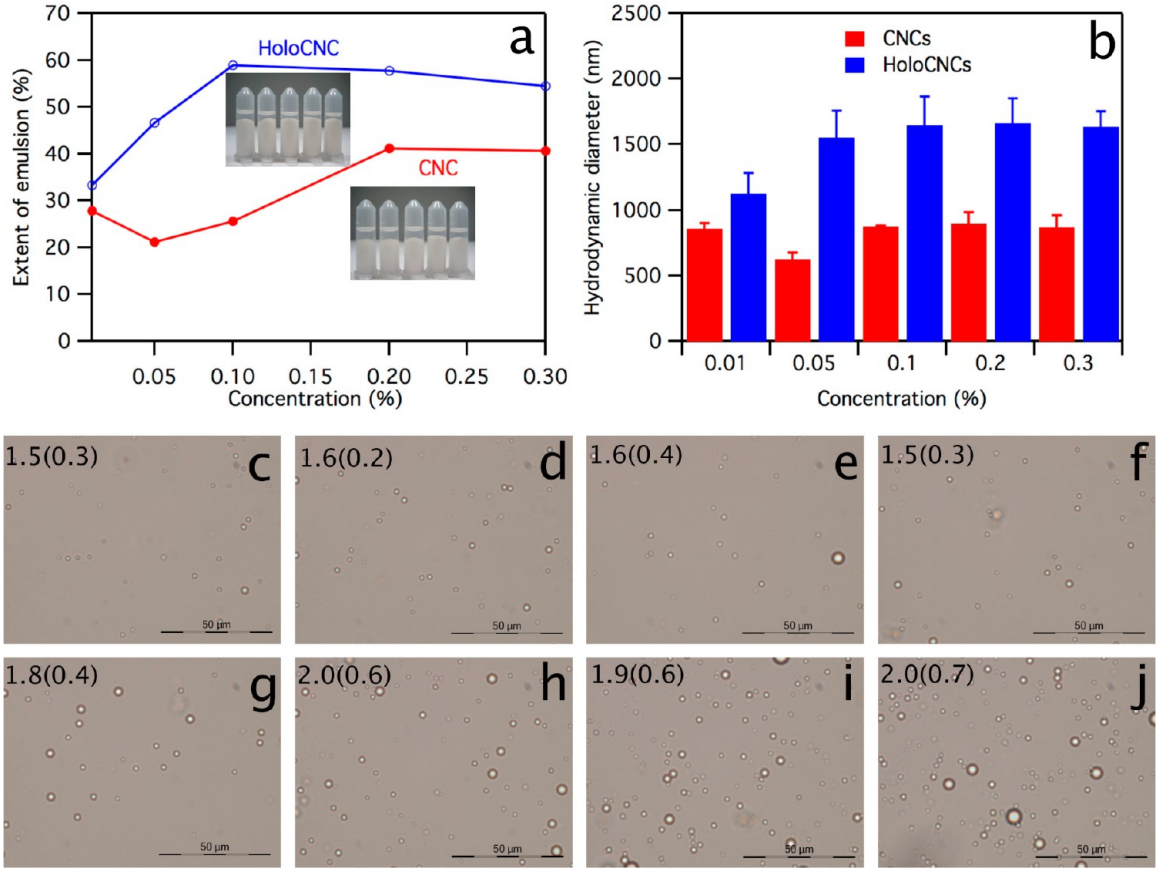

Figure 4. Pickering emulsion stabilized by CNCs and holoCNCs: (a) extent of emulsion, (b) hydrodynamic diameters, (c–j) optical microscopy CNCs (c–f) and holoCNCs (g–j) stabilized Pickering emulsions at 0.01 (c, g), 0.1 (d, h), 0.2 (e, i), and 0.3% (f, j). The average droplet diameters (standard deviation) in μm indicated in the images c–j.

I_1/I_3 value of pyrene emission spectrum is around 1.8 in water and 0.6 in hydrocarbons.[52,53] For CNCs, the I_1/I_3 values remained at around 1.8 at up to 0.1%, then decreased very slightly to 1.7 at 0.2% (Figure 3a). Although the cellulose chain is considered amphiphilic, that is, hydrophilic equatorial hydroxyls and hydrophobic axial CH in the glucopyranose ring, aqueous CNCs behave essentially as polar molecules like water, exhibiting I_1/I_3 of 1.8 at up to 0.1%. The slightly lowered I_1/I_3 values at above 0.1% suggest some association of CNCs along the equatorial hydroxyls via hydrogen bonding to expose more of the hydrophobic axial CHs. In contrast, the I_1/I_3 is 1.77 for pyrene in 0.0001% holoCNCs, slightly lower than the 1.80 for water or in CNCs at the same concentration, suggesting holoCNCs to be less polar than CNCs, possibly due to the more hydrophobic aromatic rings of lignosulfonate on holoCNCs. The I_1/I_3 gradually decreased to 1.69 in 0.02% holoCNCs, indicating increased hydrophobicity with increasing holoCNC concentrations. The I_1/I_3 values then sharply lowered to 1.35 at 0.2% holoCNCs, suggesting 0.02% to be the onset concentration for holoCNC to form aggregated structure. The less charged holoCNCs are thought to also contain more hydrophobic lignosulfonate aromatic rings on their surfaces, leading to greater tendency to aggregate to minimize interaction with water by enclosing their hydrophobic moieties. Therefore, compared to CNCs, holoCNCs could form more hydrophobic microenvironment to host pyrene

DOI: 10.1021/acs.biomac.5b00240
Biomacromolecules 2015, 16, 1433–1441

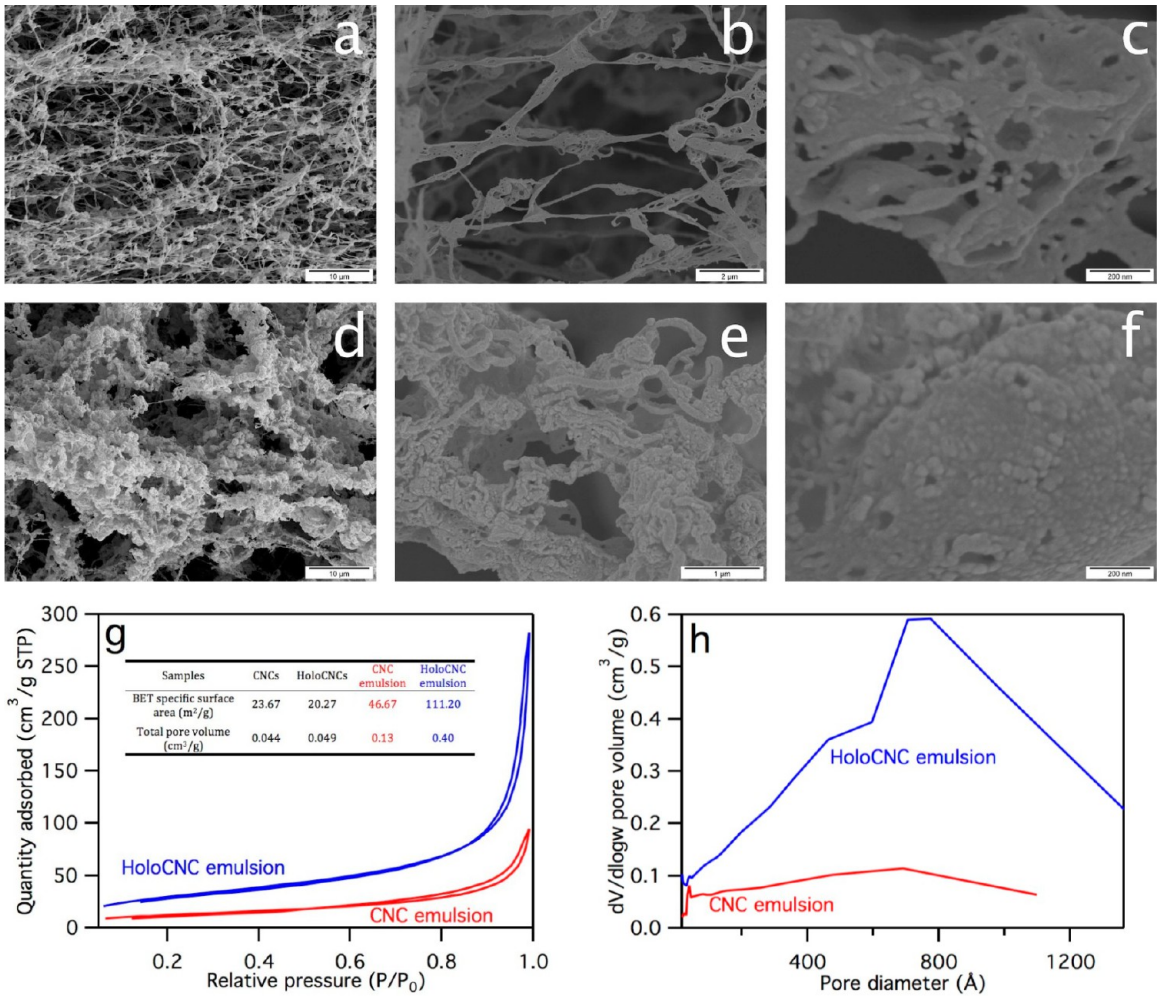

Figure 5. SEM of assembled structures by freeze-drying Pickering emulsion stabilized by 0.2% of CNCs (a–c) and holoCNCs (d–f). BET isotherm (g) and pore size distribution (h) of freeze-dried 0.2% CNC and holoCNC emulsions. Inset in (g) is specific surface area and total pore volume.

molecules. Although the 1.35 I_1/I_3 value for holoCNCs is significantly lower than the 1.7 I_1/I_3 value for CNCs, this value is still higher than the 0.86 I_1/I_3 value for sodium dodecyl sulfate (SDS),[53] suggesting inferior surface active properties of holoCNCs as compared to commercial surfactant.

The surface tensions of aqueous CNC suspension were around 71.8 mN/m at below 0.1% (Figure 3b), close to that (72.75 mN/m at 20 °C) of pure water,[54] then lowered to 67.1 mN/m at 1%, indicating CNCs to be slightly amphiphilic and consistent with the steady-state fluorescence results. The surface tensions of aqueous holoCNC suspensions, on the other hand, decreased drastically at dilute concentrations, from 72.1 mN/m at 0.00025% to 68.3 mN/m at 0.005%, further decreased to 50.3 at 0.4% and finally reached a near constant 49.2 mN/m at above 0.4%. The more significant and continuously decreasing surface tensions with increasing holoCNC concentrations indicate aggregates formation with the critical aggregation concentration (CAC) of 0.57% determined from the intersection of the two fitting curves.

While TEMPO oxidized CNCs have previously shown to lower the equilibrium surface tension to 53 mN/m,[43] the 49.2 mN/m equilibrium surface tension of surface active holoCNCs is lower and the first reported from direct sulfuric acid hydrolysis without additional surface modification. This holoCNC surface tension is slightly higher than those of surface modified CNCs, such as poly[2-(dimethylamino)ethyl methacrylate]-grafted-CNCs (47 mN/m)[42] and Jeffamine-grafted oxidized CNCs (41 mN/m),[43] but has the advantage of being from far more efficiently isolated and without additional reactions. Both fluorescence probe and surface tension analysis indicate holoCNCs to be more highly amphiphilic than CNCs, exhibiting surface active behavior by lowering the equilibrium surface tension of water to 49.2 mN/m and forming aggregates at above CAC of 0.57%.

Pickering Emulsion Stabilization of HoloCNCs and CNCs. The ability of holoCNCs and CNCs in stabilizing O/W Pickering emulsions was evaluated in 3/7 v/v hexadecane/water. Biphasic solution with a top oil layer was formed upon adding hexadecane to aqueous suspensions containing 0.01 to 0.3% holoCNCs and CNCs. Upon sonication, the transparent aqueous layer turned into creamy opaque O/W emulsion, leaving remaining oil as a transparent layer on the top (inset, Figure 4a). The extent of emulsion increased from 33 to 59% with increasing holoCNC concentrations from 0.01 to 0.1%, then remained at 59% at up to 0.3% (Figure 4a). In contrast, the extent of emulsion first decreased from 28 to 21% as the CNC concentration increases from 0.01 to 0.05%, then increased to 41% with increasing CNC concentration to 0.2%, and remained constant at 0.3% CNC. While both holoCNCs and CNCs could stabilize Pickering emulsions, the

DOI: 10.1021/acs.biomac.5b00240
Biomacromolecules 2015, 16, 1433–1441

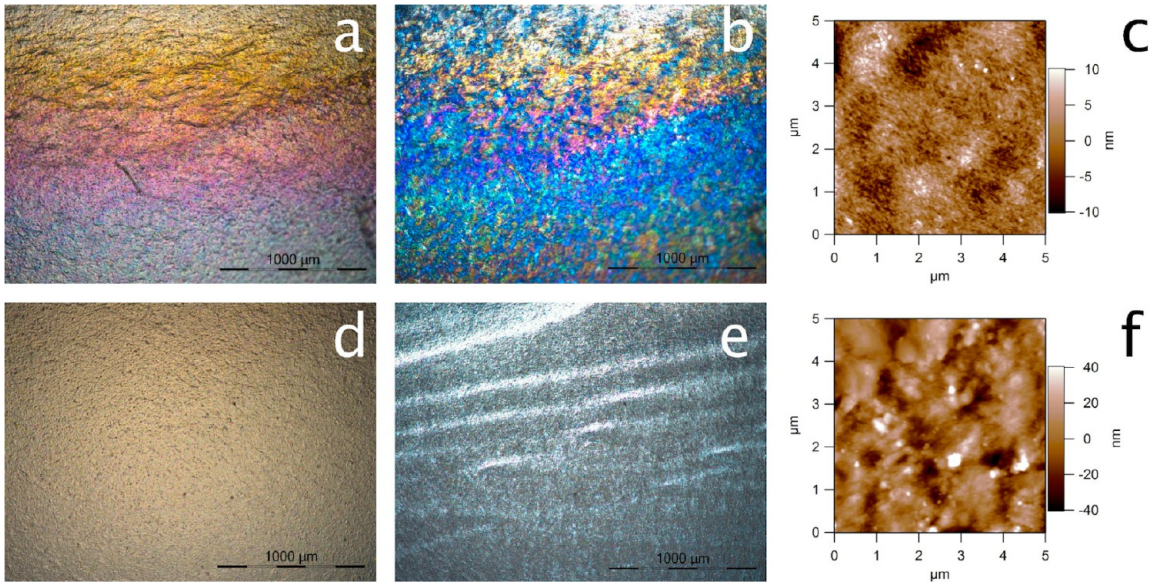

Figure 6. Films casted from 2% aqueous CNC (a–c) and holoCNC (d–f) suspensions: light microscope images (a, d) without and (b, e) with cross-polarizer, and (c, f) AFM height image.

maximum extent of emulsion for holoCNCs (59%) is significantly higher than that of CNCs (41%) and the holoCNC concentration (0.1%) needed for maximal emulsion is half of CNC concentration (0.2%). Besides, the emulsions formed with holoCNCs remain stable for at least 3 weeks, far longer than the CNC-stabilized emulsions that completely disappeared in 4 days. All of these indicate holoCNCs to be much better emulsifiers. The better stability of holoCNCs in stabilizing Pickering emulsion could be ascribed to the increased hydrophobicity from surface adsorbed lignosulfonate aromatic rings, improving amphiphilicity. Besides, the less charged holoCNCs could also shift toward stronger inter holoCNC association and away from hydrophilic interaction with water to stabilize the O/W interfaces, as highly charged CNCs have been known to reversibly desorb from the oil/water interface, except when the negative charge groups are removed by desulfation or screened by increasing ionic strength.[55,56]

The hydrodynamic diameters of the emulsion droplets in holoCNCs stabilized emulsions were 1.2–1.6 μm, double in sizes (0.6–0.8 μm) of those in CNC stabilized emulsions (Figure 4b). The significantly larger hydrodynamic diameters of emulsion droplets stabilized with holoCNCs are further proof to their greater hydrophobicity to stabilize more oil. Besides, the hydrodynamic diameters stayed almost constant over concentrations for both CNC and holoCNC, except for that with 0.01% holoCNCs, indicating emulsion droplet sizes to be independent of nanocellulose concentrations. The optical microscope images further showed more numerous droplets in holoCNC emulsions (Figure 4g–j) than in the CNC counterparts (Figure 4c–f), consistent with the higher extent of holoCNC emulsions. The holoCNC emulsions contained droplets in 1.8–2.0 μm average diameters, as determined from light microscope, approximately 25% larger than the 1.5–1.6 μm droplet sizes in CNC emulsions, with neither sizes being concentration-dependent. However, the numbers of droplets increased with higher 0.1–0.3% holoCNCs, showing the quantities of the emulsion droplets to be concentration dependent. The larger droplet sizes by light microscope than DLS may be due to the compression between the cover and glass slides. Therefore, droplet dimensions determined by DLS were deemed more accurate.

Self-Assembling Behaviors of HoloCNCs and CNCs. The ability of holoCNCs and CNCs to assemble was observed from the structure they freeze- and air-dried into porous mass and cast film, respectively. The creamy emulsions stabilized by 0.2% CNC and holoCNC were rapidly frozen in liquid nitrogen then freeze-dried into respective white and pale brown fluffy mass, consistent with the colors of their aqueous suspensions. Both showed highly porous structures (Figure 5a–f). The freeze-dried CNC emulsion showed predominantly thin submicron wide fibers interspersed with highly isolated micron sized hollow clusters (Figure 5a–c). The distinct fiber and hollow cluster morphologies are thought to assembled from CNCs suspended in aqueous phase and those adsorbed on the oil droplets, respectively. The greater extent of fibers than hollow clusters is clearly evident of most CNCs being in aqueous phase, indicative of more hydrophilic nature of CNCs and consistent with the lower extent of emulsion stabilized by CNCs. The clusters, with sizes vary from 0.5 to 1.4 μm and close to the hydrodynamic diameters of the emulsion droplets, are hollow inside with CNC outer shells but not in perfect spherical shape (Figure 5c), possibly due to the sublimation of entrapped hexadecane during freeze-drying. In contrast, holoCNCs assembled into more clusters but little fibers (Figure 5d–f), and the surface of clusters are more densely packed as compared to the loosely packed CNC clusters (Figure 5c), all consistent with their higher surface active role at the O/W droplet interfaces. Closer inspection on the holoCNCs clusters showed them to be about 2 μm sizes, much bigger than those from CNCs, and consistent with the hydrodynamic diameters of the holoCNC stabilized emulsion droplets.

Both BET nitrogen adsorption of freeze and freeze-dried holoCNC and CNC O/W emulsions showed typical type IV isotherms with a narrow hysteresis loops containing nearly parallel type H1 adsorption and desorption branches (Figure 5g), indicating meso- and macroporous structures. These are in

DOI: 10.1021/acs.biomac.5b00240
Biomacromolecules 2015, 16, 1433–1441

contrast to the type II isotherms with nearly reversible adsorption and desorption loops from those freeze-dried from their aqueous suspensions, typical of nonporous or macroporous structures (Figure S3, Supporting Information). The porous structures from freezing and freeze-drying of CNCs and holoCNCs O/W emulsions had significantly higher specific surface of 46.67 and 111.20 m^2/g as well as total pore volume of 0.13 and 0.40 cm^3/g (inset, Figure 5g), respectively, than their respective structures from aqueous suspensions (23.67 and 20.27 m^2/g specific surface, 0.044 and 0.049 cm^3/g pore volume, respectively). Besides, pore size distribution curves for both holoCNC and CNC emulsions showed pore width ranging from 10 to 120 nm, centering at around 70−80 nm (Figure 5h), confirming the presence of meso- and macropores. The newly observed meso- and macroporosity with increased specific surface and pore volume in both cases are clearly associated with their O/W emulsions, that is, reduced self-assembly during freeze-drying due to adsorption at the oil/water interfaces, which are consistent with SEM observation. During freeze-drying, the nanocrystals at the oil−water interfaces could be dried into porous structures, whereas the isolated nanocrystals in aqueous phase would assembled with each other to form nonporous fibers and films. While the specific surface and pore volume increased by 2 and 3 times for CNCs, the increase for holoCNCs was impressively higher at 3 and 8 times, respectively. The much higher specific surface and pore volume of holoCNCs than CNCs are clearly related to the more adsorbed holoCNCs at the oil−water interfaces and their more heterogeneous surfaces and less ability to assemble.

Self-assembly behaviors of holoCNC and CNC during air-drying were also investigated by casting respective films from 2% aqueous suspensions. The CNC film showed iridescent colors, indicative of a chiral nematic structure (Figure 6a,b) that reflects left-handed circularly polarized light in visible range,[57−59] typical of the phase-separated ordered chiral nematic liquid crystal phase above critical concentration.[57,60] During slow evaporation, CNCs concentrate to above the critical concentration to self-assemble into chiral nematic liquid crystalline form, which was retained upon solidification in the film. In contrast, lacking chiral nematic iridescence in the holoCNC films indicates absence of orderly chiral nematic liquid crystalline form (Figure 6d,e). The AFM of CNC film showed well aligned CNCs while holoCNC film surface appeared more heterogeneous with no individually identifiable holoCNCs, indicating all the crystalline cellulose was buried with amorphous lignosulfonate/hemicellulose phases (Figure 6c,f). The few bright dots observed were likely from the residual silica particles. HoloCNC film also showed a significantly higher root-mean-square (RMS) roughness of 13.9 nm than the much smoother CNC film whose 3.2 nm RMS is slightly higher but comparable roughness to the 1.4−2.5 nm roughness of spin-coated CNC model films.[12,61,62] The lack of iridescence color and less-defined structures of holoCNCs but rougher surfaces suggested the rod-like holoCNCs could not be aligned during the slow drying process, possibly due to the presence of heterogeneous components, such as amorphous lignosulfonate, hemicellulose, and silica, that interfere with the self-assembly of holoCNCs.

CONCLUSIONS

Holocellulose and α-cellulose were isolated from rice straw following a two-step dewax-delignification process and an additional alkaline leaching to 36.4 and 75.4% yield, respectively. HoloCNCs and CNCs were then derived via sulfuric acid hydrolysis (64%, 45 °C, 45 min) at 11.6 and 6.8% yield of holocellulose and α-cellulose or 8.8 and 2.5% of rice straw, respectively. HoloCNCs were similar in lateral dimensions to, but slightly shorter and less homogeneous (4.1 ± 1.6 nm thick, 6.4 ± 1.8 nm wide and 113 ± 70 nm long) than, CNCs (4.7 ± 1.3 nm thick, 6.4 ± 1.2 nm wide and 143 ± 31 nm long). While the presence of lignosulfonate, hemicellulose, silica, and sulfur in holoCNCs was confirmed by FTIR, EDS, and UV−vis, CNCs were pure cellulose. HoloCNCs were also less charged (0.128 mmol/g) and crystalline (84.4%) than CNCs (0.237 mmol/g, 90.7%), but had much higher maximum mass loss temperature of 284 °C than that (235 °C) of CNCs. Most strikingly is the better surface active behavior of holoCNCs, as revealed by their foaming ability and amphiphilicity from steady-state fluorescence showing the decreased pyrene emission I_1/I_3 value to 1.35 at 0.2%, absent for CNCs. HoloCNCs also lower the equilibrium surface tension significantly to 49.2 mN/m at above CAC of 0.57% as compared to the slightly lowered surface tension to 67.1 mN/m for 1% CNCs. Both CNCs and holoCNCs were capable of forming 3/7 O/W Pickering emulsions, but that with holoCNCs was 30% more emulsified and their emulsion droplets were double in sizes than that with CNCs. Furthermore, while both O/W emulsions could be freeze-dried to form more porous structure than their aqueous counterparts, that from holoCNCs had significantly higher specific surfaces and pore volumes, clearly evident of their higher hydrophobicity and lesser ability to self-assemble from the oil−water interfaces. These uniquely surface active, amphiphilic, and less self-assembling properties of holoCNCs offer desirable characteristics that had only been obtainable by additional and often elaborate surface modification of CNCs. It is also advantageous that holocellulose took one step less to isolate than pure cellulose.

ASSOCIATED CONTENT

Supporting Information

FTIR and TGA of α-cellulose and holocellulose. FTIR and EDS of residuals from sulfuric acid hydrolyzed holocellulose. BET isotherm of freeze-dried 0.2% CNC and HoloCNC suspensions. This material is available free of charge via the Internet at http://pubs.acs.org.

AUTHOR INFORMATION

Corresponding Author

*E-mail: ylhsieh@ucdavis.edu. Fax: +1 530 752 7584. Tel.: +1 530 752 0843.

Notes

The authors declare no competing financial interest.

ACKNOWLEDGMENTS

The authors appreciate the assistance of Darren Dinh on the optical microscopic observation of O/W droplets in Pickering emulsions and surface tension measurement and Paul Hrvatin in Chemistry at UC Davis for his dedicated support in providing access to the fluorescence spectrometer as well as the funding support by the California Rice Research Board (Project RU-9).

REFERENCES

(1) Lin, N.; Huang, J.; Dufresne, A. *Nanoscale* **2012**, *4*, 3274−3294.

DOI: 10.1021/acs.biomac.5b00240
Biomacromolecules 2015, 16, 1433−1441

(2) Klemm, D.; Kramer, F.; Moritz, S.; Lindstrom, T.; Ankerfors, M.; Gray, D.; Dorris, A. *Angew. Chem., Int. Ed.* **2011**, *50*, 5438−5466.
(3) Habibi, Y.; Lucia, L. A.; Rojas, O. J. *Chem. Rev.* **2010**, *110*, 3479−3500.
(4) Moon, R. J.; Martini, A.; Nairn, J.; Simonsen, J.; Youngblood, J. *Chem. Soc. Rev.* **2011**, *40*, 3941−3994.
(5) Beck-Candanedo, S.; Roman, M.; Gray, D. G. *Biomacromolecules* **2005**, *6*, 1048−1054.
(6) Jiang, F.; Esker, A. R.; Roman, M. *Langmuir* **2010**, *26*, 17919−17925.
(7) Jiang, F.; Hsieh, Y.-L. *Carbohydr. Polym.* **2013**, *95*, 32−40.
(8) Lu, P.; Hsieh, Y. L. *Carbohydr. Polym.* **2012**, *87*, 564−573.
(9) Iwamoto, S.; Kai, W. H.; Isogai, A.; Iwata, T. *Biomacromolecules* **2009**, *10*, 2571−2576.
(10) Matsuo, M.; Sawatari, C.; Iwai, Y.; Ozaki, F. *Macromolecules* **1990**, *23*, 3266−3275.
(11) Saito, T.; Kuramae, R.; Wohlert, J.; Berglund, L. A.; Isogai, A. *Biomacromolecules* **2013**, *14*, 248−253.
(12) Jiang, F.; Kittle, J. D.; Tan, X.; Esker, A. R.; Roman, M. *Langmuir* **2013**, *29*, 3280−3291.
(13) Roman, M.; Winter, W. T. *Biomacromolecules* **2004**, *5*, 1671−1677.
(14) Lu, P.; Hsieh, Y. L. *Carbohydr. Polym.* **2010**, *82*, 329−336.
(15) Dong, X. M.; Revol, J.-F.; Gray, D. G. *Cellulose* **1998**, *5*, 19−32.
(16) Favier, V.; Chanzy, H.; Cavaille, J. Y. *Macromolecules* **1995**, *28*, 6365−6367.
(17) Angles, M. N.; Dufresne, A. *Macromolecules* **2000**, *33*, 8344−8353.
(18) Capadona, J. R.; Shanmuganathan, K.; Trittschuh, S.; Seidel, S.; Rowan, S. J.; Weder, C. *Biomacromolecules* **2009**, *10*, 712−716.
(19) Jiang, F.; Hsieh, Y.-L. *Carbohydr. Polym.* **2013**, *95*, 32−40.
(20) Rosa, S. M. L.; Rehman, N.; de Miranda, M. I. G.; Nachtigall, S. M. B.; Bica, C. I. D. *Carbohydr. Polym.* **2012**, *87*, 1131−1138.
(21) Lu, P.; Hsieh, Y. L. *Carbohydr. Polym.* **2012**, *87*, 2546−2553.
(22) Helbert, W.; Cavaille, J. Y.; Dufresne, A. *Polym. Compos.* **1996**, *17*, 604−611.
(23) Jiang, F.; Hsieh, Y.-L. *Carbohydr. Polym.* **2015**, *122*, 60−68.
(24) Chen, D.; Lawton, D.; Thompson, M. R.; Liu, Q. *Carbohydr. Polym.* **2012**, *90*, 709−716.
(25) Mueller, S.; Weder, C.; Foster, E. J. *RSC Adv.* **2014**, *4*, 907−915.
(26) Himmel, M. E.; Ding, S. Y.; Johnson, D. K.; Adney, W. S.; Nimlos, M. R.; Brady, J. W.; Foust, T. D. *Science* **2007**, *315*, 804−807.
(27) Iiyama, K.; Lam, T. B. T.; Stone, B. A. *Plant Physiol.* **1994**, *104*, 315−320.
(28) Iwamoto, S.; Abe, K.; Yano, H. *Biomacromolecules* **2008**, *9*, 1022−1026.
(29) Arola, S.; Malho, J.-M.; Laaksonen, P.; Lille, M.; Linder, M. B. *Soft Matter* **2013**, *9*, 1319−1326.
(30) Spence, K. L.; Venditti, R. A.; Habibi, Y.; Rojas, O. J.; Pawlak, J. J. *Bioresour. Technol.* **2010**, *101*, 5961−5968.
(31) Milanovic, J.; Kostic, M.; Milanovic, P.; Skundric, P. *Ind. Eng. Chem. Res.* **2012**, *51*, 9750−9759.
(32) Puangsin, B.; Fujisawa, S.; Kuramae, R.; Saito, T.; Isogai, A. *J. Polym. Environ.* **2013**, *21*, 555−563.
(33) Okita, Y.; Saito, T.; Isogai, A. *Holzforschung* **2009**, *63*, 529−535.
(34) Mao, L. S.; Law, K.; Claude, D.; Francois, B. *Ind. Eng. Chem. Res.* **2008**, *47*, 3809−3812.
(35) Meng, Q.; Li, H.; Fu, S.; Lucia, L. A. *React. Funct. Polym.* **2014**, *85*, 142−150.
(36) Kuramae, R.; Saito, T.; Isogai, A. *React. Funct. Polym.* **2014**, *85*, 126−133.
(37) Bras, J.; Hassan, M. L.; Bruzesse, C.; Hassan, E. A.; El-Wakil, N. A.; Dufresne, A. *Ind. Crops Prod.* **2010**, *32*, 627−633.
(38) Rosa, M. F.; Medeiros, E. S.; Malmonge, J. A.; Gregorski, K. S.; Wood, D. F.; Mattoso, L. H. C.; Glenn, G.; Orts, W. J.; Imam, S. H. *Carbohydr. Polym.* **2010**, *81*, 83−92.
(39) Hu, Z.; Sarah, B.; Robert, P.; D, C. E. *J. Colloid Interface Sci.* **2015**, *439*, 139−148.
(40) Heux, L.; Chauve, G.; Bonini, C. *Langmuir* **2000**, *16*, 8210−8212.
(41) Visanko, M.; Liimatainen, H.; Sirviö, J. A.; Heiskanen, J. P.; Niinimäki, J.; Hormi, O. *Biomacromolecules* **2014**, *15*, 2769−2775.
(42) Tang, J. T.; Lee, M. F. X.; Zhang, W.; Zhao, B. X.; Berry, R. M.; Tam, K. C. *Biomacromolecules* **2014**, *15*, 3052−3060.
(43) Azzam, F.; Heux, L.; Putaux, J. L.; Jean, B. *Biomacromolecules* **2010**, *11*, 3652−3659.
(44) Segal, L.; Creely, J. J.; Martin, A. E., Jr.; Conrad, C. M. *Text. Res. J.* **1959**, *29*, 786−794.
(45) Brunauer, S.; Emmett, P. H.; Teller, E. *J. Am. Chem. Soc.* **1938**, *60*, 309−319.
(46) Barrett, E. P.; Joyner, L. G.; Halenda, P. P. *J. Am. Chem. Soc.* **1951**, *73*, 373−380.
(47) Van Soest, P. J. *Anim. Feed Sci. Technol.* **2006**, *130*, 137−171.
(48) Binod, P.; Sindhu, R.; Singhania, R. R.; Vikram, S.; Devi, L.; Nagalakshmi, S.; Kurien, N.; Sukumaran, R. K.; Pandey, A. *Bioresour. Technol.* **2010**, *101*, 4767−4774.
(49) Wexler, A. S. *Anal. Chem.* **1964**, *36*, 213−&.
(50) Li, H.; Liu, H.; Fu, S. Y.; Zhan, H. Y. *Bioresources* **2011**, *6*, 1681−1695.
(51) Kim, S.; Silva, C.; Zille, A.; Lopez, C.; Evtuguin, D. V.; Cavaco-Paulo, A. *Polym. Int.* **2009**, *58*, 863−868.
(52) Kalyanasundaram, K.; Thomas, J. K. *J. Am. Chem. Soc.* **1977**, *99*, 2039−2044.
(53) Turro, N. J.; Lei, X. G.; Ananthapadmanabhan, K. P.; Aronson, M. *Langmuir* **1995**, *11*, 2525−2533.
(54) Vargaftik, N. B.; Volkov, B. N.; Voljak, L. D. *J. Phys. Chem. Ref. Data* **1983**, *12*, 817−820.
(55) Kalashnikova, I.; Bizot, H.; Cathala, B.; Capron, I. *Langmuir* **2011**, *27*, 7471−7479.
(56) Kalashnikova, I.; Bizot, H.; Cathala, B.; Capron, I. *Biomacromolecules* **2012**, *13*, 267−275.
(57) Beck, S.; Bouchard, J.; Chauve, G.; Berry, R. *Cellulose* **2013**, *20*, 1401−1411.
(58) Cheung, C. C. Y.; Giese, M.; Kelly, J. A.; Hamad, W. Y.; MacLachlan, M. J. *ACS Macro Lett.* **2013**, *2*, 1016−1020.
(59) Giese, M.; De Witt, J. C.; Shopsowitz, K. E.; Manning, A. P.; Dong, R. Y.; Michal, C. A.; Hamad, W. Y.; MacLachlan, M. J. *ACS Appl. Mater. Interfaces* **2013**, *5*, 6854−6859.
(60) Beck, S.; Bouchard, J.; Berry, R. *Biomacromolecules* **2011**, *12*, 167−172.
(61) Kittle, J. D.; Du, X.; Jiang, F.; Qian, C.; Heinze, T.; Roman, M.; Esker, A. R. *Biomacromolecules* **2011**, *12*, 2881−2887.
(62) Kittle, J. D.; Wondraczek, H.; Wang, C.; Jiang, F.; Roman, M.; Heinze, T.; Esker, A. R. *Langmuir* **2012**, *28*, 11086−11094.

DOI: 10.1021/acs.biomac.5b00240
Biomacromolecules 2015, 16, 1433−1441